Energy & Environmental Science

A Sobering Examination of the Feasibility of Aqueous Aluminum Batteries

Journal:	*Energy & Environmental Science*
Manuscript ID	EE-ART-01-2022-000134.R2
Article Type:	Paper
Date Submitted by the Author:	13-Apr-2022
Complete List of Authors:	Pastel, Glenn; Army Research Laboratory, Battery Sciences Branch Chen, Ying; Pacific Northwest National Laboratory Pollard, Travis P.; Army Research Laboratory, Battery Sciences Branch Schroeder, Marshall; Army Research Laboratory, Battery Sciences Branch Bowden, Mark; Pacific Northwest National Laboratory Zheng, Allen; Hunter College CUNY Hahn, Nathan; Sandia National Laboratories Ma, Lin; US Army Research Laboratory, Battery Sciences Branch Murugesan, Vijayakumar; Pacific Northwest National Laboratory Ho, Janet; Army Research Laboratory, Battery Sciences Branch Garaga, Mounesha; Hunter College CUNY Borodin, Oleg; Army Research Laboratory, Battery Sciences Branch Mueller, Karl; Pacific Northwest National Laboratory Greenbaum, Steve; Hunter College CUNY, Physics Xu, Kang; Army Research Laboratory, Battery Sciences Branch

ARTICLE

A Sobering Examination of the Feasibility of Aqueous Aluminum Batteries

Received 17th January 2022,
Accepted 00th March 2022

DOI: 10.1039/x0xx00000x

Glenn R. Pastel,‡[a] Ying Chen,‡[b] Travis P. Pollard,‡[a] Marshall A. Schroeder,[a] Mark E. Bowden,[b] Allen Zheng,[c] Nathan T. Hahn,[d] Lin Ma,[a] Vijayakumar Murugesan,[b] Janet Ho,[a] Mounesha Garaga,[c] Oleg Borodin,[a] Karl Mueller,*[b] Steven Greenbaum,*[c] and Kang Xu*[a]

Aqueous aluminum (Al) batteries are posited to be a cheap and energy dense alternative to conventional Li-ion chemistries, but an aqueous electrolyte mediating trivalent aluminum cations (Al^{3+}) warrants greater scrutiny. This study provides a rigorous examination of aqueous Al electrolytes, with the first compelling evidence for a dynamic octahedral solvation structure around the Al^{3+}, without Al-OTf contact ion pairs, even at high concentrations. This solvation behavior and the concomitant, transient electrostatic hydrolysis of Al-OH_2 ligands contrasts strongly with previously reported water-in-salt electrolytes, and occurs due to the high charge density of the Lewis acidic Al^{3+}. Nuclear magnetic resonance spectroscopy and other physicochemical measurements quantitatively reveal how species activity evolves with concentration and temperature. This new understanding exposes practical concerns related to the corrosiveness of the acidic aqueous solutions, the degree of hydration of aluminum trifluoromethanesulfonate ($Al(OTf)_3$) salt, and the grossly insufficient reductive stability of the proposed electrolytes (>1 V between HER onset and Al^{3+}/Al). Collectively, these factors constitute multiple fundamental barriers to the feasibility of rechargeable aqueous Al batteries.

INTRODUCTION

Rechargeable Al-ion and Al-metal (Al^{3+}/Al^{0}) batteries represent appealing multivalent chemistries due to the high theoretical capacity of the trivalent redox reaction (Al ↔ $Al^{3+} + 3e^{-}$, 8040 mAh mL^{-1}), the relatively low reduction potential (-1.667 V vs. SHE), and high abundance of Al in the earth's crust.[1–3] However, realizing these properties in practical devices is contingent on addressing the fundamental challenges associated with solvating Al^{3+} in the electrolyte, transporting them across interfaces, and hosting them in cathode materials.[4] The high oxidation state and high charge density of Al^{3+} present a strong impediment to all of these processes.[5] Additionally, Al has a high oxide bonding energy (502 kJ mol^{-1}), which leads to aggressive passivation of Al^{0} surfaces in the presence of radical oxygen and water. Therefore, there have been few, if any, full cell demonstrations that profit from the theoretical energy density associated with the three-electron transfer of Al^{3+}/Al redox.

a. Battery Sciences Branch, U.S. Army Research Laboratory, Adelphi, Maryland 20783, United States.
b. The Joint Center for Energy Storage Research (JCESR), Pacific Northwest National Laboratory, Richland, WA 99354, USA.
c. Department of Physics & Astronomy, Hunter College of the City University of New York, New York, NY 10065 USA.
d. The Joint Center for Energy Storage Research (JCESR), Sandia National Laboratories, Albuquerque, NM 87123, USA.
* Corresponding author(s)
‡ G.R.P., Y.C., and T.P.P. contributed equally to this work.
Electronic Supplementary Information (ESI) available: [details of any supplementary information available should be included here]. See DOI: 10.1039/x0xx00000x

Recently, high gravimetric energy densities above 400 Wh kg^{-1} have been claimed for MnO_2‖Al full cells with impressive cycling metrics. However the reported chemistry closely resembles voltaic cells from the 1950s with unresolved corrosion issues.[6–9] Past prototypes used either halide or caustic alkaline based electrolytes, which both suffer from fatal trade-offs. Aluminum halides tend to form dimer complexes that act as an anolyte in fiercely corrosive solutions or molten salts, thereby imposing high electrolyte loading requirements and reducing commercial viability. Alkaline systems can provide high power density but have negligible reversibility and are limited to primary battery applications.[10] On a fundamental level, the discovery of novel aluminum electrolytes has been hampered by the extremely high Lewis acidity of the trivalent cation, which introduces challenges not only during synthesis of the salt precursor and electrolyte solution, but also with the reversibility of electrochemical processes. Recent reports based on aluminum trifluoromethanesulfonate in aqueous media ($Al(OTf)_3$-H_2O) offer promising cycling stability by eliminating the native alumina layer and re-passivating with deep eutectic solvents. However, there is limited evidence that contact ion pairing and solvation behaviour enables reversible Al^{3+} redox in these highly concentrated aqueous solutions, as well as skepticism that these chloroaluminate passivation layers are long-lived.[11,12] Therefore, there is an urgent need to clarify the key challenges associated with aqueous aluminum electrolytes, which represent one of the cheapest and most energy dense solutions for next-generation battery technologies.

Lewis acids, including aluminum trifluoromethanesulfonate ($Al(OTf)_3$), have been widely applied in organic synthesis as catalysts with favourable selectivity and reactivity under mild conditions.[13,14] However, a complete understanding of the associated catalytic reactions has been obfuscated by the solvation structure of the catalytic species. Specifically, the tightly bound trihydrate ligands of $Al(OTf)_3$ revealed in this work play an unknown role in the first solvation shell of Al^{3+} which governs the performance in nonaqueous media. In this study, nuclear magnetic resonance (NMR) spectroscopy serves as a critical tool for deconvoluting the solvation structure of $Al(OTf)_3$-H_2O solutions by identifying likely solvate interactions. Yet, the full implications of the tightly bound trihydrate and solvation structure on various catalytic reactions might still require additional investigation beyond the scope of this work.
Super-concentrated electrolytes are known to bring about unexpected bulk liquid structures, ion transport, and interfacial properties when the cations are monovalent.[15] Whether such benefits could be replicated for multivalent cations remains unknown. While improvements have been noted in super-concentrated zinc (Zn) electrolytes, the large radius (75 pm) and soft Lewis acidity of Zn^{2+}, due to its d-orbitals, significantly reduces the Coulombic field strength within its solvation sheath.[16] As such, the effect of solvation structure on suppressing the hydrogen evolution reaction (HER) at low reduction potentials is pronounced for both aqueous lithium- and zinc-based electrolytes,[17,18] while an opposing trend was observed in this study for aluminum-based electrolyte. In this work, we delve into the solvation structure and redox reactions of $Al(OTf)_3$-H_2O solutions to determine their utility for rechargeable aluminum batteries. We tentatively hypothesized that concentration and pre-treatment methods would not sufficiently hinder hydrogen evolution when attempting to reversibly strip and plate aluminum in $Al(OTf)_3$-H_2O. Our experiments indicate earlier onset of HER with increasing concentration and other trends stemming from the solvation structure of the Al^{3+} cation in aqueous electrolyte. Conditions to enable reversible Al^{3+} redox in protic solvents are proposed for the first time; future work will need to carefully sidestep misleading and competing chemical as well as electrochemical processes.

RESULTS AND DISCUSSION

Thermodynamic Considerations. A Pourbaix diagram represents Nernstian predictions of the equilibria among the solid and solution phases in an aqueous system with known pH and electrochemical potential.[19] Although reaction and interfacial kinetics are neglected, these diagrams establish useful guidelines regarding the competition between deposition, corrosion, and passivation in aqueous solutions. In Figures 1c and 1d, the unshaded regions of the Pourbaix diagram for soluble monomeric Al species indicate high reactivity of Al^0 and the Al_2O_3 passivation layer under acidic conditions below a pH of 2.5. In this study, these conditions were realized in corrosion tests with aqueous $Al(OTf)_3$ solutions of at least 1 m concentration (Figure S1). Al^0 rapidly corrodes

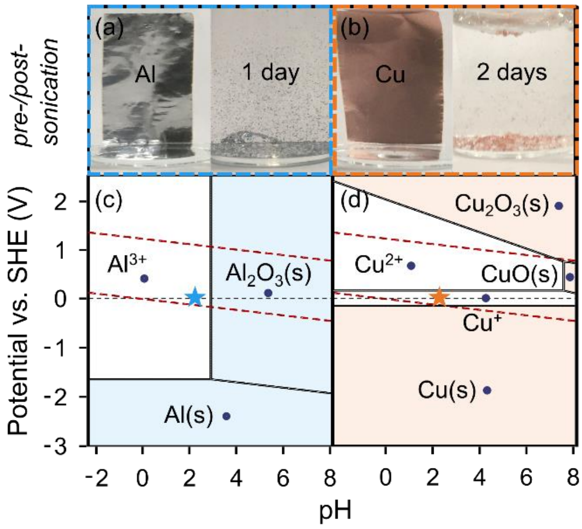

Figure 1. (a-b) Images of aluminum and copper metal before and after sonicating in 1 m $Al(OTf)_3$-H_2O for 1 and 2 days, respectively. (c) Pourbaix diagrams of 1 M aluminum and (d) 10^{-8} M copper in aqueous media at 25 °C. The dotted red lines represent the thermodynamic stability of water, regions where solid phases dominate are shaded, and the initial conditions of the corrosion tests correspond to the starred points on the diagram. Both diagrams were extracted from the Materials Project.

and amphoteric $Al(OH)_3(H_2O)_3$ dissociates under open circuit potentials in the acidic solution (Figure 1a). The formation of ε-Keggin ions and other multimeric nanoscale clusters can be ruled out due to the low pH of the solution.[19,20] This result indicates that Al^0 must be passivated, beyond its native alumina layer, before it can be used as an anode in $Al(OTf)_3$-H_2O electrolyte.
Additional corrosion tests with various metals indicate similar behaviour without any sign of adequate passivation. For instance, the corrosion of copper, a common current collector material, leads to a noticeable change in colour associated with $[Cu(H_2O)_6]^{2+}$ complexes under open circuit conditions (Figure 1b and S2). As a result, although commonly used in Li metal cycling and anode-free configurations, copper is unsuitable for aqueous $Al(OTf)_3$-H_2O without sufficient protection by the interface.
To avoid side reactions of the substrate or electrode material in subsequent tests, inert precious metals are relied upon to evaluate the properties of the $Al(OTf)_3$-H_2O electrolyte as few other metals are stable under the expected pH and electrochemical window for aqueous Al electrolytes. Future work should prioritize careful evaluation of electrode-electrolyte stability, given the Lewis acidity of Al^{3+} cations.
Hydration. $Al(OTf)_3$ from multiple sources contained water as determined by attenuated total reflectance Fourier transform infrared spectroscopy (ATR-FTIR), thermal analysis by differential scanning calorimetry (DSC) and thermogravimetric analysis coupled with mass spectroscopy (TGA-MS), as well as Karl Fisher titration in rigorously dried non-aqueous solvents. ATR-FTIR of the salt prepared in a dry atmosphere and measured under a sealed anvil revealed O-H stretching bands and hydrogen bonding between water molecules in a tetrahedral "ice-like" structure at 3343 and 3245 cm^{-1},

respectively.[21] This structure is lost after exposure to a humid environment, as the hygroscopic salt absorbs ambient moisture from a room with greater than thirty percent relative humidity within minutes (Figure S3).

Less than one weight percent mass loss was observed by TGA-MS of dry $Al(OTf)_3$ salt between room temperature and 200 °C, indicating the stability of bound water in the crystal structure of the salt (Figure S4). DSC further confirms an irreversible endothermic event just above 200 °C. After this event, the salt has been decomposed into an amorphous glass, most likely dominated by alumina, as identified from *ex-situ* XRD (Figure S5). This behaviour is strongly reminiscent of the fate of $AlCl_3·6H_2O$ and other hygroscopic salts, from which crystalline water cannot be removed by thermal desorption or chemical dehydration. From multiple coulometric titrations in a nonaqueous solvent of known water content, the most likely stoichiometry of the hydrate is $Al(OTf)_3·3H_2O$ (528 amu), with at least three water molecules bound per Al^{3+} (Figure S6 and Table S1). Synthesis methods under anhydrous conditions with neat H(OTf) and triakyl Al precursors are likely necessary to realize dehydrated $M(OTf)_3$ salts. However, further studies along these lines are beyond the scope of the current work.[22] Previous studies noted a solubility limit of $Al(OTf)_3$ in aqueous media around 5 M (mol L^{-1}) at 25 °C, and this value drops to 2.1 M or 3.6 m (mol kg^{-1}), after accounting for the hydration content of the bound trihydrate. Compared to Li-based water-in-salt systems with a solvent to cation ratio of 3:1, the $Al(OTf)_3$-H_2O solution is definitively in the "dilute" concentration regime with a ratio greater than 15:1. The lower solubility limit reduces the likelihood of localized or bulk salt contact ion pair and aggregate formation even at the highest possible concentrations, which curtails expectations for anion-derived interfacial kinetics, reduced interface solubility, and desolvation behaviour due to direct salt reduction.[23]

Solvation Structure. *SCXRD of Solvated Ions.* Single crystals of $Al(OTf)_3$ in water were obtained by slowly evaporating the solvent or lowering the temperature of a saturated solution (see Materials and Methods for more details). The structure obtained from SCXRD refinement (Figure 2a) has a stoichiometry corresponding to $Al(OTf)_3·9H_2O$. The asymmetric unit contains aluminum cations octahedrally coordinated to six

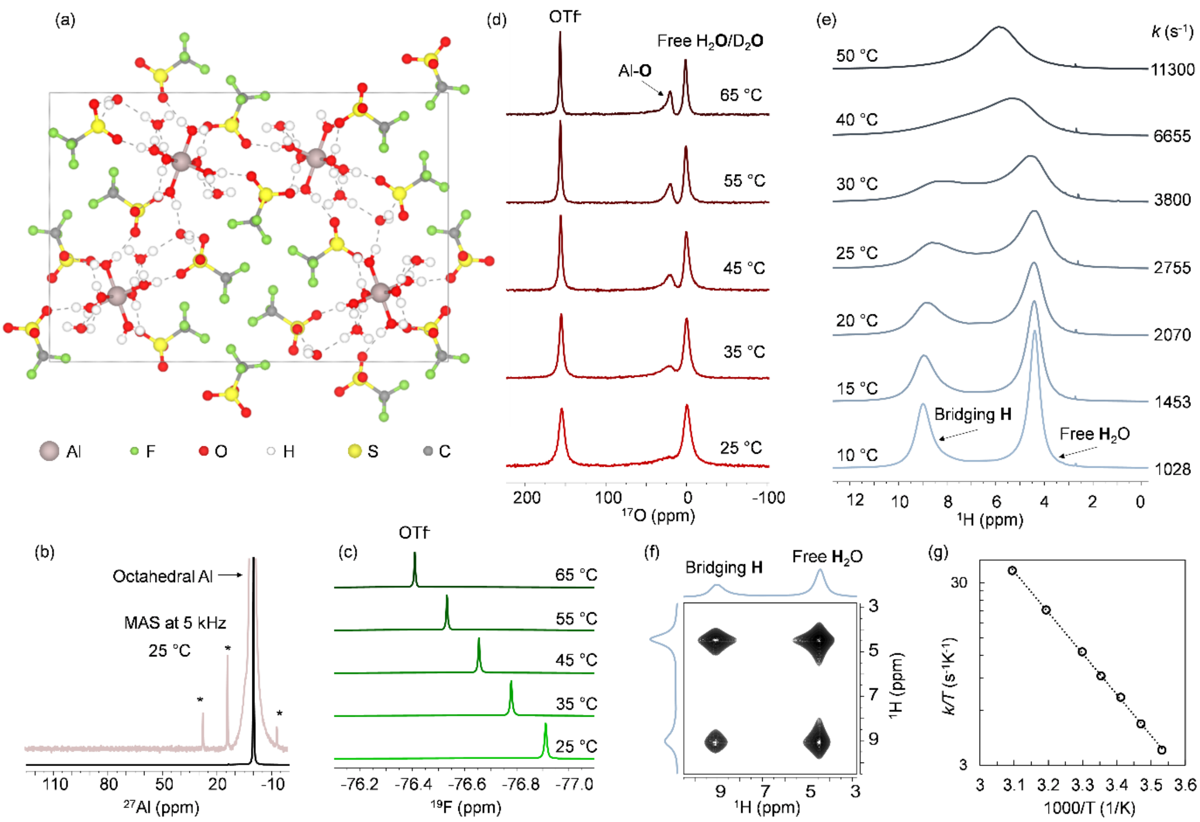

Figure 2. (a) The refined SCXRD structure of $Al(OTf)_3·9H_2O$ shows aluminum cations octahedrally coordinated to six water molecules, with three additional water molecules hydrogen-bonded to OTf^-. Al atoms are metallic pink, F green, O red, H white, S yellow, and C grey. (b-f) NMR characterization of the solvation structure of 3.6 m $Al(OTf)_3$-H_2O (for ^{27}Al and ^{17}O solid-state MAS NMR) and 3.3 m $Al(OTf)_3$-D_2O (for ^{19}F, ^{17}O and ^{1}H solution-state NMR), including: (b) ^{27}Al MAS spectrum at a spinning speed of 5 kHz showing an octahedral signal observed at around 0 ppm (black line); the zoom-in view (pink line) confirming that tetrahedral and pentahedral coordination is negligible with the spinning side bands marked with asterisks; (c) ^{19}F spectra exhibiting a single signal between 25 and 65 °C as a result of fast exchange between different OTf^- states; (d) ^{17}O spectra indicating no detectable signal for bound Al-OTf and a consistent molar fraction between bridging Al-**O**- and free H_2**O** of 2:3; (e) ^{1}H spectra indicating two distinct states, bridging **H** and **H**$_2$O with a molar fraction of 2:3; the exchange rates *k* between the two states estimated from lineshape analysis are listed at the right; (f) ^{1}H-^{1}H 2D NOESY spectrum confirming the exchange between the bridging H and free H_2O; and (g) an Eyring plot of *k*/T against 1000/T which provides the activation enthalpy of the exchange process, as calculated from the slope of the line.

water molecules with three further water molecules hydrogen bonded to the SO_3 group of OTf^- anions in the second solvation sheath. Surprisingly, no OTf^- anions form contact ion pairs with Al^{3+} in the first solvation sheath. Rather OTf^- anions form clusters which limit proximity to the Al^{3+} cation in the solid single crystals. The corresponding CIF file is included in the Supporting Information.

NMR Characterization. For additional clarity on the liquid solvation structure of potential concentrated battery electrolytes, multinuclear (^1H, ^{17}O, ^{19}F, and ^{27}Al) liquid- and solid-state NMR were performed on 3.6 m $Al(OTf)_3$-H_2O and 3.3 m $Al(OTf)_3$-D_2O solutions (2.1 M equivalence). The purpose of solid-state magic-angle-spinning (MAS) NMR is to check for large Al-O clusters with relatively slow molecular motions that are not detectable using liquid-state NMR. Previous DFT simulations suggest that the molar fraction of mononuclear species besides $Al(H_2O)_6^{3+}$ in aqueous solutions is low under acidic conditions.[25] This is supported by the ^{27}Al MAS spectrum (Figure 2b); the complete absence of signals between 30 – 120 ppm indicates negligible populations of tetrahedral and pentahedral species in these solutions.

The states of the OTf^- anions are observed by ^{19}F and ^{17}O NMR. The single ^{19}F signal (Figure 2c) and downfield ^{17}O signal at 155 ppm (Figure 2d) between 25 °C and 65 °C suggest that the exchange rates between different OTf^- states (free, contact ion pair, or solvent separated ions), if any, are much faster than the NMR spectral scale (with the fast exchange limit << 1 ms). On the other hand, ^{17}O and ^1H NMR of water both clearly reveal two distinguishable states. In addition to the free water ^{17}O signal at 0 ppm, a resonance at around 20 ppm can be assigned to the bridging O behavior of certain Al-OH_2 ligands. Deconvolution of the ^{17}O peaks shows that the molar ratio between bound water (bridging O) and free water is 2:3 over the temperature range of our study (Figure S7). From quantitative ^{17}O NMR, given that the molar ratio of total solvent to OTf^- is 1.8:1 and the stoichiometric ratio of oxygen from the OTf^- to solvent is 9:1, the molar ratio of solvent to dry salt is found to be approximately 16:1. This ratio is in near perfect agreement with the Karl Fisher titration measurements and is consistent with a salt precursor stoichiometry of $Al(OTf)_3{\cdot}3H_2O$. All of the ^{17}O signals become sharper at higher temperatures due to faster molecular mobility, but the change is most significant for the bridging O signal. This change in lineshape with temperature suggests that there is no detectable exchange between the oxygens from free and bound water at NMR time scales (with the slow exchange limit >> 1 ms). Conversely, the two well-resolved ^1H signals at 10 °C (free water at 4.4 ppm, bridging H^+/bound water at 9.0 ppm) become broader and eventually merge as the temperature increases, which is clear evidence of the exchange between protons from free and bound water (Figure 2e). The ^1H-^1H 2D NOESY spectrum also confirms the exchange between the two proton signals (Figure 2f). Lineshape analysis of the spectra yields the molar ratio and the exchange rates between the two states (Figure S8). The molar ratio between bound and free water obtained from ^1H NMR is also approximately 2:3, consistent with the value estimated from ^{17}O NMR. The calculated proton exchange rates (k) are in the range of 1,000 to 11,000 s^{-1}. An Eyring plot of k/T against 1000/T (Figure 2g) indicates an activation enthalpy of 43 kJ/mol (10 kcal/mol) for this proton exchange reaction, which is close to the bond-dissociation enthalpy of a second hydration sheath of H_3O^+.[25]

The molar ratios between solvent to salt species (16:1) and bound to free water (2:3) suggest that Al^{3+} coordinates closely to the oxygen atoms from the six water ligands in the first solvation sheath, thereby differentiating them from free water molecules. This agrees well with the local environment of Al^{3+} in the hydrated single crystals. However, unlike the stable hydrogen bonding network in the single crystals, hexa-aqua Al^{3+} in the concentrated solutions may act as Brønsted-Lowry acids, which allow their water ligands to be deprotonated by water or OTf^- outside the first solvation sheath, acting as a Brønsted-Lowry base.[26,27] These deprotonations are acid-base reactions, in which the oxidation state of the metal ion remains unchanged, while deprotonated H^+ likely travel via the Grotthuss mechanism (Figure S9).[26] This solvation behavior differs significantly from previously reported water-in-salt electrolytes and is indicative of the challenges stemming from the highly Lewis-acidic Al^{3+}.

Raman Spectroscopy. When an OTf^- forms a contact ion pair with an Al^{3+}, its symmetry is broken such that a frequency shift is expected in the nondegenerate symmetric vibrational bands, specifically the CF_3 bending (δ_S) and SO_3 stretching (ν_S) modes.[22] Shifts in the former have been captured well by recent work on zinc electrolytes, with nearly negligible blueshift at the solubility limit.[23] This led the authors to assert that negligible contact ion pairing occurs in concentrated $Zn(OTf)_2$-H_2O solutions at room temperature. Similar behaviour for the CF_3 band is observed in the $Al(OTf)_3$-H_2O system with only a weak blueshift from 766 to 768 cm^{-1}. However, a more notable blueshift of the SO_3 band above 2 m, from 1034 cm^{-1} to 1041 cm^{-1}, has resulted in contradicting assertions regarding the existence of Al-OTf contact ion pairs at high concentrations (Figure S10 & Table S2). One possible explanation for this seemingly conflicting behaviour considers contact ion pairing between hydronium cations (H_3O^+) and OTf^- in solution. To investigate this hypothesis, Raman spectroscopy was performed on dilutions of aqueous $Al(OTf)_3$ as well as triflic acid (HOTf) solutions with the same molar ratio of free triflate and unbound water (Figure 3a). Surprisingly, both solutions show a similar blueshift in the SO_3 and CF_3 bands from low to high concentrations.[24] A small shift in the CF_3 band (< 5 cm^{-1}) is observed as well as an additional mode around 1041 cm^{-1} in the SO_3 band at high concentrations in both solutions. The similar trend for the two binary solutions reduces the likelihood that the high energy SO_3 mode can be ascribed to Al-OTf contact ion pairs. Instead, the similarity in the H(OTf) and $Al(OTf)_3$ spectra is indicative of significant hydrogen bonding and proton activity in both solutions. This alternative explanation is explored further by modelling likely solvation phenomena and interactions.

Computation. Born-Oppenheimer molecular dynamics (BOMD) modelling provides additional confirmation of the formation of H_3O^+ and OTf^- ion pairs (Figure 3b). Assuming dominance of the $[Al(H_2O)_6]^{3+}$ species across all concentrations, consistent with

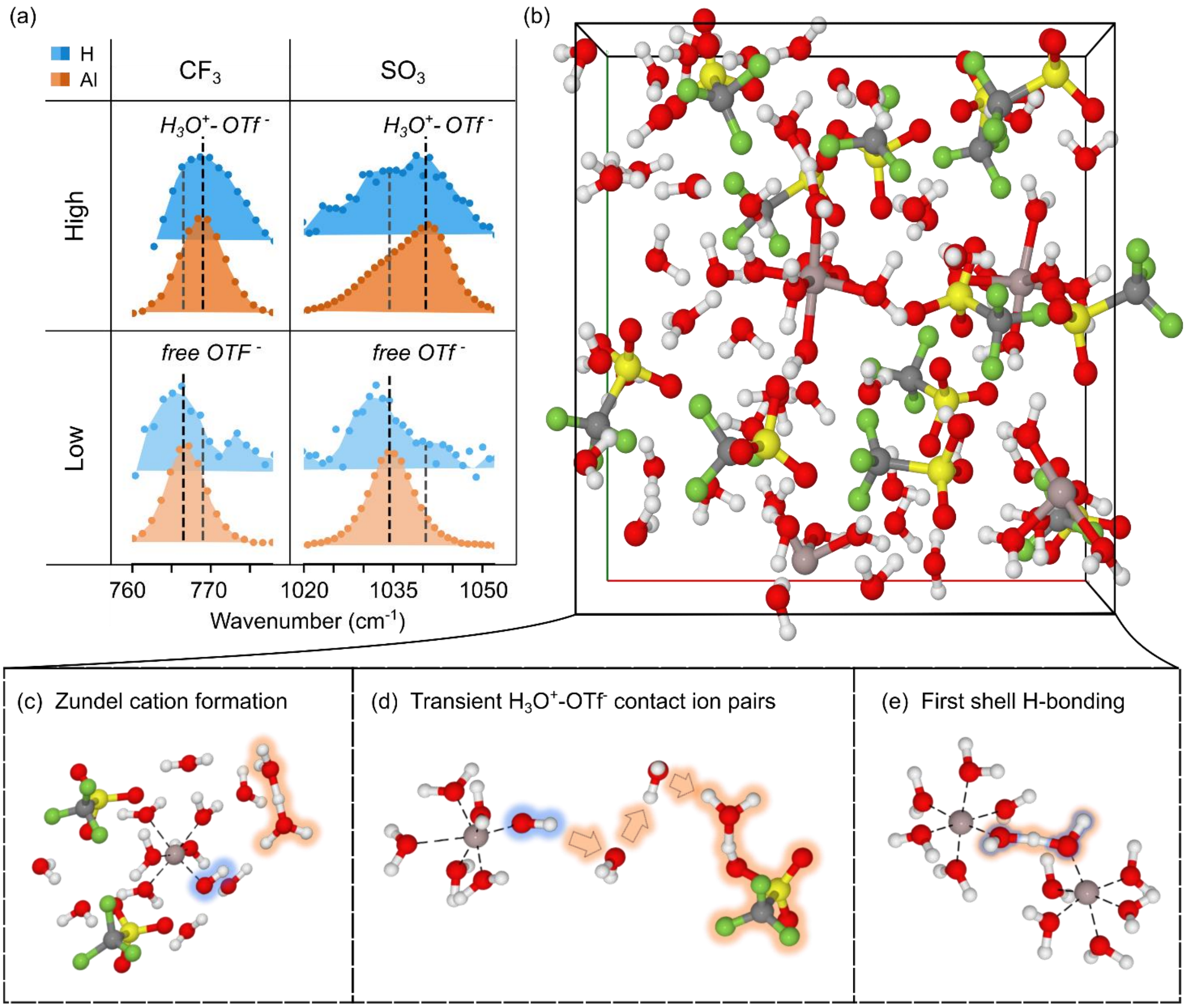

Figure 3. (a) Raman spectra of the CF_3 and SO_3 vibrational bands of H(OTf) and $Al(OTf)_3$ solutions at 20 °C. The blueshift observed from the 1.0 m to 3.6 m $Al(OTf)_3$ solutions mimics the shift between 3.4 m and 17.7 m H(OTf) solutions. The respective low and high concentration solutions have equivalent molar ratios of free OTf^- to unbound water, outside the first solvation shell of Al^{3+}. (b) A snapshot of the Born-Oppenheimer molecular dynamics simulation trajectories with insets (c-e) highlighting unique species observed throughout the simulations. A blue glow denotes Al^{3+}-bound OH and an orange glow denotes proton related species (e.g. hydronium, Zundel cation, or H_3O-OTf ion pairing). This color pairing is unrelated to the Raman spectra in (a).

the ^{27}Al NMR results, MD simulations indicate that metal-bound water ligands can release a proton. The free proton is found as either a H_3O^+ or Zundel cation ($H_5O_2^+$, Figure 3c-d) which diffuses via Grotthuss structural diffusion among neighboring water molecules until eventually reforming $[Al(H_2O)_6]^{3+}$ (in simulation). An elevated simulation temperature of 800 K was necessary to overcome the 10 kcal/mol kinetic barrier predicted by NMR to initiate this process on BOMD timescales (<100 picoseconds); Grotthuss events occur on the order of a few hundred femtoseconds at this temperature. Transient contact ion pairs between H_3O^+ and OTf^- were observed in BOMD (Figure 3d). In one of the simulation trajectories, coupling between neighboring aluminum solvation shells sheaths via tight hydrogen bonding were also observed (Figure 3e). The proton is strongly delocalized between the sheaths and rapidly passes back and forth between the OH^- species. The $[Al(H_2O)_5OH]^{2+}$ solvate structure remains octahedral consistent with the absence of resonances related to 4- or 5-coordinate Al^{3+} sheaths. Bound waters are not displaced by triflate over the length of the simulations (4 independent simulations, each for 62 ps), so no contact ion pair formation between Al^{3+} and OTf^- is observed. Static density functional theory calculations predict that the H_3O-OTf ion pair produces a similar blueshift of the SO_3 band to that observed in the Raman spectra for the $Al(OTf)_3$ and H(OTf) solutions (Figure S11). Therefore, there is strong evidence that H_3O-OTf ion pairs are responsible for the phenomena that once masqueraded as solvates with much improved cathodic stability.

Transport Properties. Pulsed field gradient (PFG) NMR of ^{27}Al, ^{19}F, and ^{1}H was performed to measure the self-diffusion

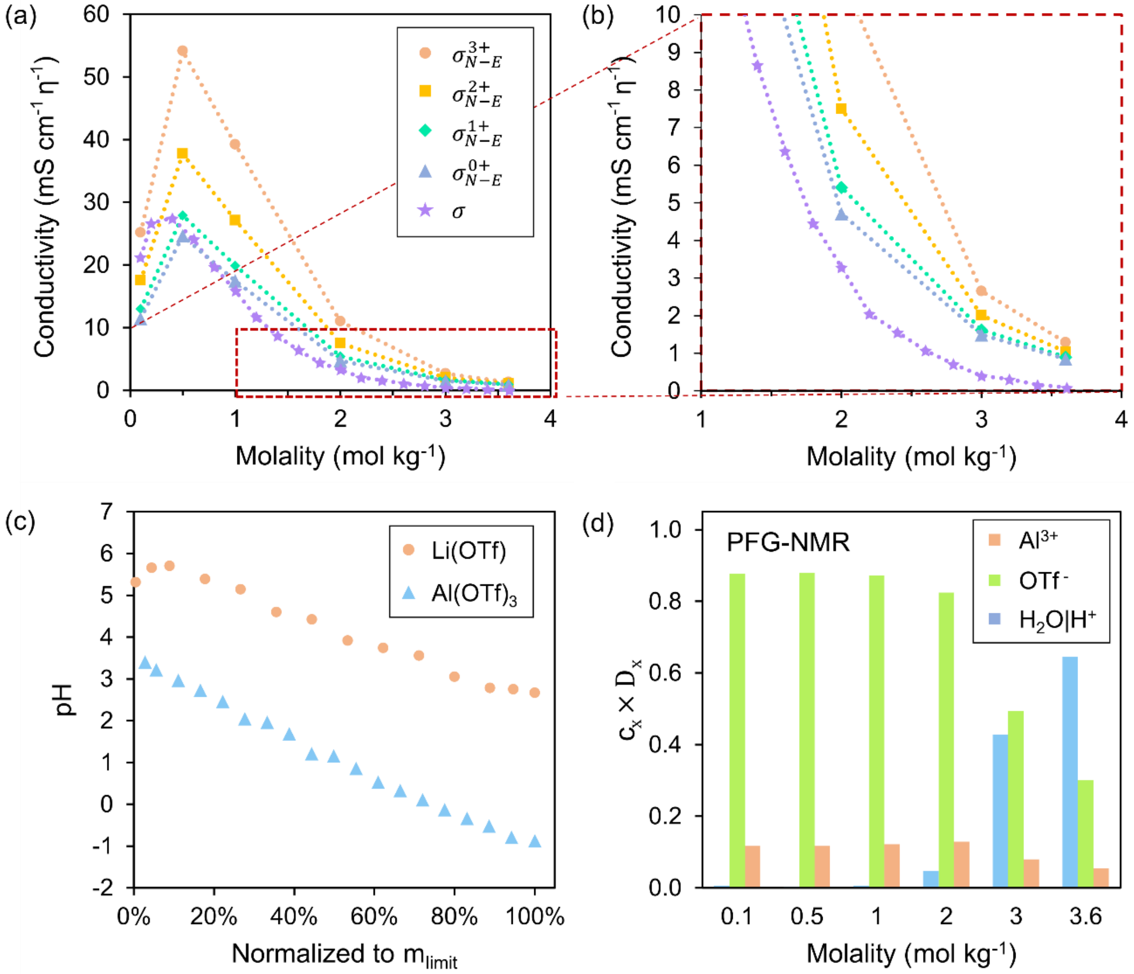

Figure 4. (a, b) Ionic conductivity of $Al(OTf)_3$-H_2O solutions predicted from PFG-NMR diffusivity measurements with various Al complex oxidation states compared to the measured conductivity (purple) and normalized against the viscosity with respect to molality. (c) pH of $Al(OTf)_3$-H_2O and Li(OTf)-H_2O solutions with respect to concentration, normalized against the solubility limit (3.6 and 22.5 m, respectively). (d) The ratios of the product of ion concentration and diffusivity as a function of molality, interpreted from PFG-NMR with the molar concentration of H^+ approximated from a classical interpretation of pH.

coefficients of Al^{3+}, OTf^-, and H^+, respectively, and derive ionic conductivity via the Nernst-Einstein (NE) relation (Figure S12). For solutions with concentrations below 0.5 m, the NE-derived conductivities agree well with the measured conductivities. However, at higher concentrations, agreement between the derived and measured conductivity is improved substantially by assuming an abundance of aluminum solvates with lower oxidation states (Figure 4a). According to experimental observations, these solvates are most likely either solvent-separated ion pairs (SSIPs) or water ligands that readily release protons and act as bound OH^- in the first solvation sheath. Dielectric relaxation spectroscopy provides some evidence for solvent-separated ion pairs of the form $[Al(H_2O)_6(OTf)]^{2+}$ and $[Al(H_2O)_6(OTf)_2]^+$ at high concentrations (Figure S13). Evidence of deprotonated water ligands in solvates such as $[Al(H_2O)_5OH]^{2+}$ exists from Raman and BOMD analysis. These species effectively lower the oxidation state of the cation and lead to decreased ionic conductivity in solution. Taking into account HOTf formation at high concentrations further decreases the NE estimates of conductivity, bringing them closer to the measured values (Figure S14). Again, the existence of $Al(OH)_4^-$ species and other monomeric species with a negative charge are ruled out due to the acidity of the electrolyte. Greater clarity regarding the role and existence of specific solvates is the focus of subsequent investigation.

Proton activity was investigated through pH measurements of the $Al(OTf)_3$-H_2O and Li(OTf)-H_2O systems (Figure 4c and S15). Although the pH of the latter varied significantly with time, likely due to formation of anion-rich inner Helmholtz layer on the glass pH electrode,[27] the values measured after immersing for one minute provide a similar trend (Figure S16). In both systems, a linear correlation is generally observed between pH and concentration ($R^2 \approx 0.995$ for $Al(OTf)_3$-H_2O), thereby revealing a power correlation between salt concentration and proton activity. Assuming that proton activity relates directly to proton concentration, the molar ratio of free protons capable of proton conduction is three times greater than the molar concentration of Al^{3+} cations (7.4 M vs. 2.1 M). By looking at the ratio of concentration and diffusivity normalized against all other charged species, the overall contribution of proton activity in the system becomes more apparent (Figure 4d). From this observation, it is reasonable to predict that proton activity dominates transport as well as electrochemical performance, particularly in the high concentration regime of the $Al(OTf)_3$-H_2O electrolyte. Furthermore, the formation of transient neutral complexes, such as $[HOTF]^0$, reduces the conductivity relative to NE estimates from the self-diffusion coefficients.

Electrochemical stability. Anodic and cathodic potential sweeps provide insight into the opposing trends in electrochemical stability between $Al(OTf)_3$- and Li(OTf)-H_2O solutions. Hydrolysis is suppressed in the lithium-based water-in-salt electrolytes by reducing the amount of free water available and forming a hydrophobic barrier at the interfaces. Scans of the Li(OTf) solutions (Figure 5) align with expectations with a 900 mV widening of the electrochemical window between the 1 and 22.5 m solutions. Notably, both HER and oxygen evolution reaction (OER) are delayed in the Li-based system due to the thermodynamic and kinetic effects of increasing the salt concentration (Figure S17).

In strong contrast, the $Al(OTf)_3$-H_2O system demonstrates only a 110 mV widening of the electrochemical window between 1.0 and 3.6 m. Furthermore, while the onset of OER is delayed, HER occurs even earlier at higher concentrations, with only a 230 mV overpotential from the standard reduction potential. This behaviour agrees with the shift in cell potential predicted by the Nernst equation due to changes in pH. Therefore, this effect accounts for an approximately 177 mV shift in HER and OER onset potentials due to a drop in proton activity by three orders of magnitude (59 mV pH^{-1}). Density functional theory predictions of the HER onset potential (vs Ag/AgCl) from $[Al(H_2O)_6]^{3+}$ clusters also support this observation: 0.37 V (ε=78) < 0.52 V (ε=35) < 0.71 V (ε=20). The dielectric constant was decreased to approximate an increase in salt concentration, which is justified by the dielectric relaxation spectroscopy measurements (Figure S13).

The absence of a stable interface after the first cycle leads to conditioning of the Pt electrode in the second cycle and few kinetic barriers to HER (Figure S18). Therefore, triflate reduction at lower potentials is insufficient to mitigate the interfacial reactivity and enable stable aluminum stripping and plating. This behaviour agrees well with the expectations derived from the solvation structure and acidity of the high concentration solution. It is also further confirmed by unsuccessful attempts to strip and plate appreciable capacities of aluminum in a custom-built optical cell (Figure S19). Although there are few unbound waters in the concentrated $Al(OTf)_3$-H_2O solutions, the hexa-aqua ion $[Al(H_2O)_6]^{3+}$ leads to very high proton activity and poor cathodic stability.

In the 1 m $Al(OTf)_3$-H_2O solution, it is possible to delineate the contributions from acidic species to the reduction current versus free water hydrolysis. At lower concentrations, with proton activity three orders of magnitude lower than at the solubility limit (as indicated by pH), free water hydrolysis is dominant around -1 V vs. Ag/AgCl at high current densities, similar to the more neutral Li(OTf)-H_2O system. Future efforts to enable Al^{3+}/Al redox in mildly acidic aqueous solutions will require a more substantial kinetic barrier to the reduction of free water and acidic species. By increasing the salt

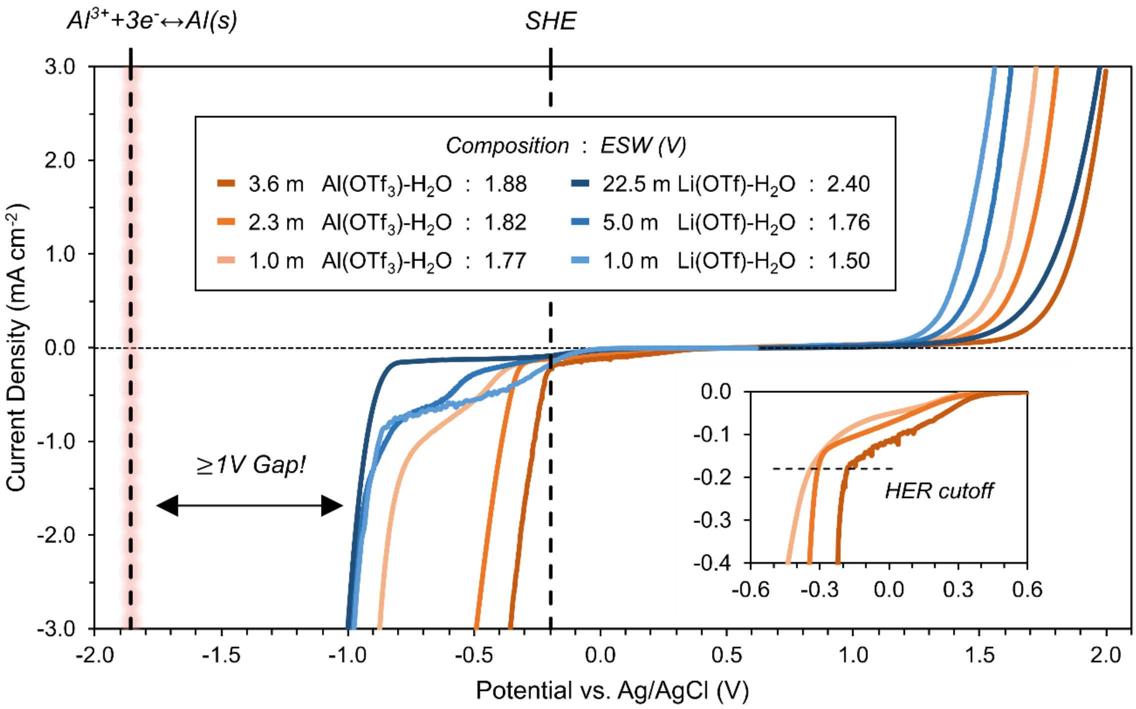

Figure 5. Linear sweep voltammetry at 5 mV sec^{-1} of $Al(OTf)_3$-H_2O and Li(OTf)-H_2O solutions in beaker cells with platinum working, Ag/AgCl reference, and glassy carbon counter electrodes. A cutoff current of 0.18 and 0.07 mA cm^{-2} is applied to both the cathodic and anodic potential sweeps, respectively, to determine the electrochemical stability window. The standard reduction potentials of aluminum and the standard hydrogen electrode at 25 °C are indicated by black dashed lines at -1.859 and -0.197 V vs. Ag/AgCl, respectively.

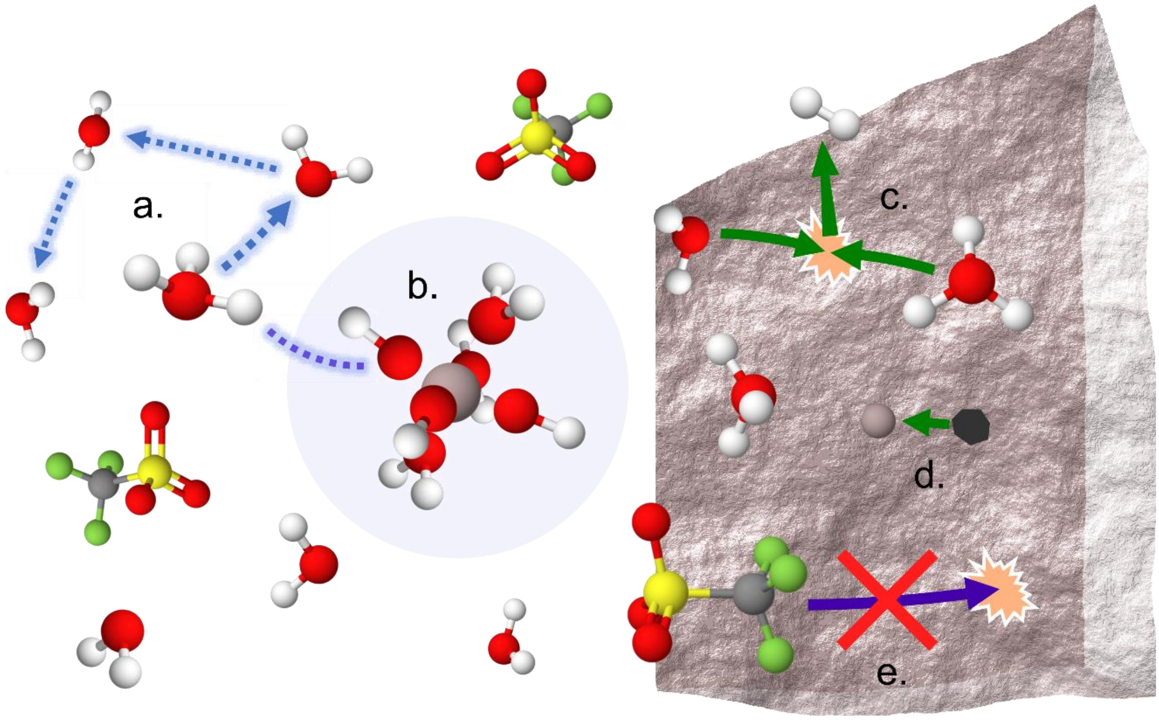

Schematic 1. The expanded solvation environment at the room temperature, solubility limit and the corresponding parasitic reactions pathways in the aqueous aluminum electrolyte, including: (a) high proton activity, (b) octahedral coordination of H_2O and transient OH^- to Al^{3+}, (c) hydrogen evolution, (d) corrosion, and (e) lack of solid electrolyte interphase formation. The aluminum substrate is the same metallic pink as the aluminum cations, in accordance with the CPK color scheme.

concentration, but failing to impede proton activity and form an anion-derived interphase, the $Al(OTf)_3$ aqueous electrolyte becomes more susceptible to HER, as predicted by the Nernst equation.

Evaluating the electrochemical stability of $Al(OTf)_3$-H_2O solutions with substrates that are susceptible to corrosion themselves is inadvisable. However, voltammetry scans of aluminum electrodes after various surface pre-treatments were performed to evaluate the corresponding artificial solid electrolyte interphases. Lower overpotentials for HER are observed after etching in 0.5 M HCl and chloride-based deep eutectic solutions, as recently confirmed in the literature (Figure S20).[33,34] Electrochemical impedance spectroscopy also indicates reduced interfacial impedance, likely due to thinning of the alumina passivation layer, which leads to an earlier onset of HER. Future research will need to consider the reduction reactions occurring in symmetric cell configurations to avoid conflating low overpotentials with improved reduction of the desired species.

Schematic 1 provides an overview of the most important challenges associated with aqueous aluminum electrolyte, including: (a) high proton activity, (b) octahedral coordination of OH^- and H_2O, (c) hydrogen evolution, (d) corrosion, and (e) lack of solid electrolyte interphase formation. Considering these challenges and the deactivation of water molecules by the Al^{3+} solvation structure, the optimistic results reported in the literature should be re-examined rigorously. Furthermore, caution should be exercised by the research community when publishing seemingly promising battery performances of aqueous Al batteries.

CONCLUSIONS

In this study, rigorous investigation of the Al^{3+} solvation environment revealed numerous factors which call for the immediate re-examination of aqueous aluminum battery claims. Many of the substrates previously considered for aqueous aluminum batteries are susceptible to corrosion in the acidic $Al(OTf)_3$-H_2O solutions, as predicted by the Pourbaix diagram. Additionally, the Raman activity of the SO_3 band and stoichiometry of the aluminum triflate trihydrate salt are often misrepresented. The high proton activity of aqueous solutions at both low and high concentrations also presents a previously undisclosed obstacle, as elucidated by NMR, physicochemical, and transport measurements. As a result, efforts to improve the cathodic stability by leveraging higher salt concentrations of $Al(OTf)_3$ are counterproductive and promote lower overpotentials for hydrogen evolution and an insufficient electrochemical stability window for aluminum stripping and plating. These findings provide, for the first time, a sobering examination of the feasibility of aqueous aluminum batteries.

Author Contributions

Glenn R. Pastel: Conceptualization, Data curation, Formal analysis, Investigation, Project administration, Visualization, Writing; **Ying Chen**: Formal analysis, Investigation, Visualization, Writing; **Travis P. Pollard**: Data curation, Formal analysis, Investigation, Software, Visualization, Writing; **Marshall A. Schroeder**: Conceptualization, Formal analysis, Investigation, Supervision, Writing - Review; **Mark E. Bowden**: Formal analysis, Investigation; **Allen Zheng**: Formal analysis, Investigation; **Nathan Hahn**: Formal analysis, Investigation, Writing - Review; **Lin Ma**: Formal analysis, Writing - Review; **Vijayakuma Murugesan**: Formal Analysis; **Janet Ho**: Resources; **Mounesha Garaga**: Formal Analysis; **Oleg Borodin**: Resources, Supervision, Writing - Review; **Karl Mueller**: Resources, Supervision, Writing - Review; **Steven Greenbaum**: Resources, Supervision; and **Kang Xu**: Funding acquisition, Project administration, Resources, Supervision, Writing - Review.

Conflicts of interest

There are no conflicts to declare.

Acknowledgements

This research was led by researchers within the Joint Center for Energy Storage Research (JCESR), an Energy Innovation Hub funded by the U.S. Department of Energy (DOE), Office of Science, Basic Energy Sciences (BES). Additionally, support for this work by the U.S. Department of the Army and DEVCOM Army Research lab is gratefully acknowledged. G.R.P would like to acknowledge Michael Ding for DSC and conductivity measurements as well as Adelaide Nolan, David Baker, and Wesley Henderson for discussions. A.Z., M.G., and S.G. acknowledge ARL for their financial support through the cooperative agreement, "Nuclear Magnetic Resonance Spectroscopy Studies of High-Impact Battery Chemistries." Liquid- and solid-state NMR experiments were performed using EMSL (grid.436923.9), a DOE Office of Science User Facility sponsored by the Office of Biological and Environmental Research. Sandia National Laboratories is a multi-mission laboratory managed and operated by National Technology & Engineering Solutions of Sandia, LLC, a wholly owned subsidiary of Honeywell International Inc., for the U.S. Department of Energy's National Nuclear Security Administration under contract DE-NA0003525. This paper describes objective technical results and analysis. Any subjective views or opinions that might be expressed in the paper do not necessarily represent the views of the U.S. Department of Energy or the United States Government.

References

1 J. Tu, W.-L. Song, H. Lei, Z. Yu, L.-L. Chen, M. Wang and S. Jiao, *Chem. Rev.*, 2021, acs.chemrev.0c01257.
2 E. Faegh, B. Ng, D. Hayman and W. E. Mustain, *Nature Energy*, 2020, 1–9.
3 K. V. Kravchyk and M. V. Kovalenko, *Commun Chem*, 2020, **3**, 120.
4 T. Leisegang, F. Meutzner, M. Zschornak, W. Münchgesang, R. Schmid, T. Nestler, R. A. Eremin, A. A. Kabanov, V. A. Blatov and D. C. Meyer, *Front. Chem.*, 2019, **7**, 268.
5 T. Nestler, S. Fedotov, T. Leisegang and D. C. Meyer, *Critical Reviews in Solid State and Materials Sciences*, 2019, **44**, 298–323.
6 Q. Zhao, M. J. Zachman, W. I. Al Sadat, J. Zheng, L. F. Kourkoutis and L. Archer, *Sci. Adv.*, 2018, **4**, eaau8131.
7 C. Wu, S. Gu, Q. Zhang, Y. Bai, M. Li, Y. Yuan, H. Wang, X. Liu, Y. Yuan, N. Zhu, F. Wu, H. Li, L. Gu and J. Lu, *Nat Commun*, 2019, **10**, 73.
8 C. Yan, C. Lv, L. Wang, W. Cui, L. Zhang, K. N. Dinh, H. Tan, C. Wu, T. Wu, Y. Ren, J. Chen, Z. Liu, M. Srinivasan, X. Rui, Q. Yan and G. Yu, *J. Am. Chem. Soc.*, 2020, **142**, 15295–15304.
9 M. J. Park, H. Yaghoobnejad Asl and A. Manthiram, *ACS Energy Lett.*, 2020, **5**, 2367–2375.
10 B. J. Hopkins, Y. Shao-Horn and D. P. Hart, *Science*, 2018, **362**, 658–661.
11 United States, US2554447A, 1951.
12 United States, US2783292A, 1957.
13 A. Cullen, 331.
14 S. Kobayashi, M. Sugiura, H. Kitagawa and W. W.-L. Lam, *Chem. Rev.*, 2002, **102**, 2227–2302.
15 O. Borodin, J. Self, K. A. Persson, C. Wang and K. Xu, *Joule*, 2020, **4**, 69–100.
16 F. Wang, O. Borodin, T. Gao, X. Fan, W. Sun, F. Han, A. Faraone, J. A. Dura, K. Xu and C. Wang, *Nature Materials*, 2018, 1.
17 R.-S. Kühnel, D. Reber and C. Battaglia, *J. Electrochem. Soc.*, 2020, **167**, 070544.
18 L. Chen, J. Zhang, Q. Li, J. Vatamanu, X. Ji, T. P. Pollard, C. Cui, S. Hou, J. Chen, C. Yang, L. Ma, M. S. Ding, M. Garaga, S. Greenbaum, H.-S. Lee, O. Borodin, K. Xu and C. Wang, *ACS Energy Lett.*, 2020, **5**, 968–974.
19 L. A. Wills, X. Qu, I.-Y. Chang, T. J. L. Mustard, D. A. Keszler, K. A. Persson and P. H.-Y. Cheong, *Nat Commun*, 2017, **8**, 15852.
20 G. Furrer, *Science*, 2002, **297**, 2245–2247.
21 F. Cheng, Q. Cao, Y. Guan, H. Cheng, X. Wang and J. D. Miller, *International Journal of Mineral Processing*, 2013, **122**, 36–42.
22 M. Chiku, S. Matsumura, H. Takeda, E. Higuchi and H. Inoue, *J. Electrochem. Soc.*, 2017, **164**, A1841–A1844.
23 L. Droguet, A. Grimaud, O. Fontaine and J.-M. Tarascon, *Advanced Energy Materials*, 2020, **10**, 2002440.
24 S. Bogatko, J. Moens and P. Geerlings, *J. Phys. Chem. A*, 2010, **114**, 7791–7799.
25 N. Agmon, *Chemical Physics Letters*, 1995, **244**, 456–462.
26 D.-W. Fong and E. Grunwald, *J. Am. Chem. Soc.*, 1969, **91**, 2413–2422.
27 J. P. Nordin, D. J. Sullivan, B. L. Phillips and W. H. Casey, *Inorg. Chem.*, 1998, **37**, 4760–4763.
28 S. Cukierman, *Biochimica et Biophysica Acta (BBA) - Bioenergetics*, 2006, **1757**, 876–885.
29 W. A. Henderson, D. M. Seo, S.-D. Han and O. Borodin, *J. Electrochem. Soc.*, 2020, **167**, 110551.
30 L. Cao, D. Li, T. Pollard, T. Deng, B. Zhang, C. Yang, L. Chen, J. Vatamanu, E. Hu, M. J. Hourwitz, L. Ma, M. Ding, Q. Li, S. Hou, K. Gaskell, J. T. Fourkas, X.-Q. Yang, K. Xu, O. Borodin and C. Wang, *Nat. Nanotechnol.*, 2021, **16**, 902–910.
31 Y. Chen, N. R. Jaegers, H. Wang, K. S. Han, J. Z. Hu, K. T. Mueller and V. Murugesan, *J. Phys. Chem. Lett.*, 2020, **11**, 6443–6449.
32 K. S. Han, Z. Yu, H. Wang, P. C. Redfern, L. Ma, L. Cheng, Y. Chen, J. Z. Hu, L. A. Curtiss, K. Xu, V. Murugesan and K. T. Mueller, *J. Phys. Chem. B*, 2020, **124**, 5284–5291.

33 T. Dong, K. L. Ng, Y. Wang, O. Voznyy and G. Azimi, *Adv. Energy Mater.*, 2021, **11**, 2100077.
34 Y. Zhang, Y. Bian, Z. Lv, Y. Han and M.-C. Lin, *ACS Appl. Mater. Interfaces*, 2021, **13**, 37091–37101.
35 E. D. Walter, L. Qi, A. Chamas, H. S. Mehta, J. A. Sears, S. L. Scott and D. W. Hoyt, *J. Phys. Chem. C*, 2018, **122**, 8209–8215.